Statistical fluctuations of transmission in slow light photonic-crystal waveguides

S. Mazoyer,[1] P. Lalanne,[1,*] J.C. Rodier,[1] J.P. Hugonin,[1] M. Spasenović,[2] L. Kuipers,[2] D.M. Beggs,[3] and T.F. Krauss[3]

[1]*Laboratoire Charles Fabry de l'Institut d'Optique, CNRS, Univ Paris-Sud, Campus Polytechnique, 91127 Palaiseau cedex, France*
[2]*Center for Nanophotonics, FOM Institute for Atomic and Molecular Physics, Science Park 104, 1098 XG, Amsterdam, The Netherlands*
[3]*School of Physics and Astronomy, University of St Andrews, St Andrews, Fife, KY169SS, UK*
**philippe.lalanne@institutoptique.fr*

Abstract: We report statistical fluctuations for the transmissions of a series of photonic-crystal waveguides (PhCWs) that are supposedly identical and that only differ because of statistical structural fabrication-induced imperfections. For practical PhCW lengths offering tolerable −3dB attenuation with moderate group indices ($n_g \approx 60$), the transmission spectra contains very narrow peaks ($Q \approx 20{,}000$) that vary from one waveguide to another. The physical origin of the peaks is explained by calculating the actual electromagnetic-field pattern inside the waveguide. The peaks that are observed in an intermediate regime between the ballistic and localization transports are responsible for a smearing of the local density of states, for a rapid broadening of the probability density function of the transmission, and bring a severe constraint on the effective use of slow light for on-chip optical information processing. The experimental results are quantitatively supported by theoretical results obtained with a coupled-Bloch-mode approach that takes into account multiple scattering and localization effects.

OCIS codes: (130.2790) Guided waves; (130.5296) Photonic crystal waveguides; (220.4241) Nanostructure fabrication; (290.4210) Multiple scattering; (999.9999) Slow light transport; (999.9999) Disorder induced losses; (999.9999) Anderson localization; (999.9999) Coupled-mode theory.

References and links

1. M. Soljacić, and J. D. Joannopoulos, "Enhancement of nonlinear effects using photonic crystals," Nat. Mater. **3**(4), 211–219 (2004).
2. M. Notomi, K. Yamada, A. Shinya, J. Takahashi, C. Takahashi, and I. Yokohama, "Extremely large group-velocity dispersion of line-defect waveguides in photonic crystal slabs," Phys. Rev. Lett. **87**(25), 253902 (2001).
3. Y. A. Vlasov, M. O'Boyle, H. F. Hamann, and S. J. McNab, "Active control of slow light on a chip with photonic crystal waveguides," Nature **438**(7064), 65–69 (2005).
4. J. K. S. Poon, L. Zhu, G. A. DeRose, and A. Yariv, "Transmission and group delay of microring coupled-resonator optical waveguides," Opt. Lett. **31**(4), 456–458 (2006).
5. D. O'Brien, M. D. Settle, T. Karle, A. Michaeli, M. Salib, and T. F. Krauss, "Coupled photonic crystal heterostructure nanocavities," Opt. Express **15**(3), 1228–1233 (2007).
6. F. Morichetti, A. Melloni, A. Breda, A. Canciamilla, C. Ferrari, and M. Martinelli, "A reconfigurable architecture for continuously variable optical slow-wave delay lines," Opt. Express **15**(25), 17273–17282 (2007).
7. T. Baba, "Slow light in photonic crystals," Nat. Photonics **2**(8), 465–473 (2008).
8. M. Notomi, E. Kuramochi, and T. Tanabe, "Large-scale arrays of ultrahigh-Q coupled nanocavities," Nat. Photonics **2**(12), 741–747 (2008).
9. S. John, "Electromagnetic Absorption in a Disordered Medium near a Photon Mobility Edge," Phys. Rev. Lett. **53**(22), 2169–2172 (1984).
10. S. Mookherjea, J. S. Park, S.-H. Yang, and P. R. Bandaru, "Localization in silicon nanophotonic slow-light waveguides," Nat. Photonics **2**(2), 90–93 (2008).
11. J. Topolancik, B. Ilic, and F. Vollmer, "Experimental observation of strong photon localization in disordered photonic crystal waveguides," Phys. Rev. Lett. **99**(25), 253901 (2007).
12. P. Erdös, and R. C. Herndon, "Theories of electrons in one-dimensional disordered systems," Adv. Phys. **31**(2), 65–163 (1982).

#128202 - $15.00 USD Received 10 May 2010; revised 6 Jun 2010; accepted 6 Jun 2010; published 23 Jun 2010

13. C. W. J. Beenakker, "Random-matrix theory of quantum transport," Rev. Mod. Phys. **69**(3), 731–808 (1997).
14. S. Mazoyer, J. P. Hugonin, and P. Lalanne, "Disorder-induced multiple scattering in photonic-crystal waveguides," Phys. Rev. Lett. **103**(6), 063903 (2009).
15. Strictly speaking, l_c is defined for lossless transport systems, only. As shown by recent theoretical results [14], backscattering is largely dominant for $n_g>20$ in the present PhCW. The out-of-plane losses being negligible, the transmitted photons may undergo many multiple-reflections without any significant damping and the expression $\langle \ln(T) \rangle = -L/l_c$ may be used safely to evaluate the localization length.
16. E. Kuramochi, M. Notomi, S. Hughes, A. Shinya, T. Watanabe, and L. Ramunno, "Disorder-induced scattering loss of line-defect waveguides in photonic crystal slabs," Phys. Rev. B **72**(16), 161318 (2005).
17. L. O'Faolain, T. P. White, D. O'Brien, X. Yuan, M. D. Settle, and T. F. Krauss, "Dependence of extrinsic loss on group velocity in photonic crystal waveguides," Opt. Express **15**(20), 13129–13138 (2007).
18. R. J. P. Engelen, D. Mori, T. Baba, and L. Kuipers, "Two regimes of slow-light losses revealed by adiabatic reduction of group velocity," Phys. Rev. Lett. **101**(10), 103901 (2008).
19. N. Le Thomas, H. Zhang, J. Jágerská, V. Zabelin, R. Houdré, I. Sagnes, and A. Talneau, "Light transport regimes in slow light photonic crystal waveguides," Phys. Rev. B **80**(12), 125332 (2009).
20. M. Patterson, S. Hughes, S. Combrié, N. V. Tran, A. De Rossi, R. Gabet, and Y. Jaouën, "Disorder-induced coherent scattering in slow-light photonic crystal waveguides," Phys. Rev. Lett. **102**(25), 253903 (2009).
21. J. Topolancik, F. Vollmer, R. Ilic, and M. Crescimanno, "Out-of-plane scattering from vertically asymmetric photonic crystal slab waveguides with in-plane disorder," Opt. Express **17**(15), 12470–12480 (2009).
22. A. Lagendijk, and B. A. van Tiggelen, "Resonant multiple scattering of light," Phys. Rep. **270**(3), 143–215 (1996).
23. G. Lecamp, J. P. Hugonin, and P. Lalanne, "Theoretical and computational concepts for periodic optical waveguides," Opt. Express **15**(18), 11042–11060 (2007).
24. D. M. Beggs, L. O'Faolain, and T. F. Krauss, "Accurate determination of the functional hole size in photonic crystal slabs using optical methods," Photonics Nanostruct. Fundam. Appl. **6**(3-4), 213–218 (2008).
25. M. Skorobogatiy, G. Bégin, and A. Talneau, "Statistical analysis of geometrical imperfections from the images of 2D photonic crystals," Opt. Express **13**(7), 2487–2502 (2005).
26. J. P. Hugonin, P. Lalanne, T. P. White, and T. F. Krauss, "Coupling into slow-mode photonic crystal waveguides," Opt. Lett. **32**(18), 2638–2640 (2007).
27. P. Velha, J. C. Rodier, P. Lalanne, J. P. Hugonin, D. Peyrade, E. Picard, T. Charvolin, and E. Hadji, "Ultracompact silicon-on-insulator ridge-waveguide mirrors with high reflectance," Appl. Phys. Lett. **89**(17), 171121 (2006).
28. A. Gomez-Iglesias, D. O'Brien, L. O'Faolain, A. Miller, and T. F. Krauss, "Direct measurement of the group index of photonic crystal waveguides via Fourier transform spectral interferometry," Appl. Phys. Lett. **90**(26), 261107 (2007).
29. D. M. Beggs, M. A. Kaliteevski, S. Brand, R. A. Abram, D. Cassagne, and J. P. Albert, "Disorder induced modification of reflection and transmission spectra of a two-dimensional photonic crystal with an incomplete band-gap," J. Phys. Condens. Matter **17**(26), 4049–4055 (2005).
30. D. Gerace, and L. C. Andreani, "Disorder-induced losses in photonic crystal waveguides with line defects," Opt. Lett. **29**(16), 1897–1899 (2004).
31. S. Hughes, L. Ramunno, J. F. Young, and J. E. Sipe, "Extrinsic optical scattering loss in photonic crystal waveguides: role of fabrication disorder and photon group velocity," Phys. Rev. Lett. **94**(3), 033903 (2005).
32. S. G. Johnson, M. L. Povinelli, M. Soljacic, A. Karalis, S. Jacobs, and J. D. Joannopoulos, "Roughness losses and volume-current methods in photonic-crystal waveguides," Appl. Phys. B **81**(2-3), 283–293 (2005).
33. L. C. Andreani, and D. Gerace, "Light-matter interaction in photonic crystal slabs," Phys. Status Solidi, B Basic Res. **244**(10), 3528–3539 (2007).
34. B. Wang, S. Mazoyer, J. P. Hugonin, and P. Lalanne, "Backscattering in monomode periodic waveguides," Phys. Rev. B **78**(24), 245108 (2008).
35. J. Bertolotti, S. Gottardo, D. S. Wiersma, M. Ghulinyan, and L. Pavesi, "Optical necklace states in Anderson localized 1D systems," Phys. Rev. Lett. **94**(11), 113903 (2005).
36. P. Sebbah, B. Hu, J. M. Klosner, and A. Z. Genack, "Extended quasimodes within nominally localized random waveguides," Phys. Rev. Lett. **96**(18), 183902 (2006).
37. J. B. Pendry, "Symmetry and transport of waves in one-dimensional disordered systems," Adv. Phys. **43**(4), 461–542 (1994).
38. Since $I(z) = |c^+(z)|^2 - |c^-(z)|^2$ represents the net flow of energy in the positive-z direction, $I(z) - I(z + a) \approx a\, \partial I(z)/\partial z$ represents the out-of-plane loss of the unit cell located between z and $z + a$.
39. Chaotic transmission spectra that strongly depart from theory predictions are also observed with slow light in coupled-cavity systems, see Ref. 8 for instance.

1. Introduction

The group velocity of light can be controlled by material resonances, such as the sharp absorption transitions of an atomic vapour, or by material engineering, such as man-made resonant devices. The second method represents a promising solution for on-chip buffering, time-domain processing and switching of optical signals [1] and consists of synthesizing artificial materials, in which photons tunnel from one site to another, thereby incurring a

#128202 - $15.00 USD Received 10 May 2010; revised 6 Jun 2010; accepted 6 Jun 2010; published 23 Jun 2010

delay. Control over slow light may also improve the phase control in interferometric modulators and the performance of phased-array beam shapers. Since the initial observation of a 40-fold reduction of the group velocity in a Photonic-Crystal Waveguide (PhCW) [2], improvements in design and fabrication have led to a series of impressive milestones obtained with in-line devices, such as coupled ring-resonators or PhC geometries [3–8] with nanosecond delays on small ($\approx 10^2$-10^3 μm^2) footprints. However, these promising results are limited by the impact of inevitable random fabrication fluctuations on slow-light transport [9], which may eventually lead to photon localization [10,11] for intentionally large disorders.

The present work is not devoted to the study of light localization in PhCWs, but rather to understand what is the impact of disorder on the light transport in practical situations of slow light transport. Hereafter, we will refer to the terminology classically used for the electronic transport in 1D systems [12–14], distinguishing the ballistic regime that is obtained for waveguide lengths L much smaller than the localization length l_c [15], and the localization regime obtained for $L>>l_c$. More specifically, we will be concerned by the intermediate regime, $L\approx l_c$, which offers a good compromise between loss and delays.

To our knowledge, most of experimental analyses of slow light based on man-made resonances rely on measurements performed on a single device [1–7,10,11,16–21]. If we do not refer to sensitive arguments by invoking ergodicity, this actually precludes observing the fundamentals of the slow-light transport that heavily rely on ensemble averaged quantities [22] discussed here. In Section 2, we collect information on a series of 18 PhCWs that are nominally identical and that only differ by statistical structural imperfections. We consider practical situations that are typically encountered in applications, obtained for PhCWs with modest lengths ($\approx$100 μm) and modest group velocities (c/20-c/60). Importantly, in Section 3, we infer "termination-less" transmission from the transmission spectra measured in Section 2. Consistently with recent theoretical predictions [14], we observe that, even for practically-relevant devices that offer 3dB losses on average ($L\approx l_c$), the PhCW transmission strongly varies from one sample realization to another, see Section 4. By calculating and measuring the field-pattern inside the waveguide in Section 5, we further interpret this phenomenon, critical for applications of slow light, as a consequence of randomly embedded local spatial modes that are premises of the localization regime and that coexist with extended stationary-field modes with a substantial back-propagating component.

2. Photonic crystal waveguide fabrication and characterization

We have fabricated 18 PhCWs formed by a single missing row of holes in the ΓK direction of an hexagonal lattice of air holes (so-called "W1" PhCWs, as shown in Fig. 1). These 18 guides are designed to be identical and only differ by the residual imperfections left by our state-of-the-art fabrication. They were patterned into the 220nm thin silicon layer of a silicon-on-insulator substrate using electron beam lithography. The positions of the air holes are fixed in a hexagonal array with a lattice constant a = 420 nm and a hole radius $r = 0.3a$. Once the holes were etched with a chlorine-based inductively coupled plasma reactive ion etching into a 220-nm-thick silicon layer, the buried oxide layer was removed with a hydrofluoric acid solution forming a free standing PhC slab. The band structure of the fundamental Bloch mode is shown in the top inset of Fig. 1. It has been calculated with a Fourier Bloch-Mode Method [23] for geometric parameters directly measured on the waveguide [24]. For $a/\lambda\approx 0.27$, the fundamental Bloch mode exhibits anomalous dispersion: the group velocity (calculated as $d\omega/dk$) gradually decreases as the wavevector approaches the Brillouin zone boundary ($\lambda\approx$1560 nm). As illustrated in the scanning electron microscope (SEM) image in Fig. 1, the 185a-long waveguides are connected to 3-mm-long ridge access waveguides. Additionally and very importantly for the following analysis, the ridge-to-PhCW interfaces incorporate a fast-slow transition that enables efficient injection, even for group velocities as low as $10^{-2}c$ [26].

#128202 - $15.00 USD Received 10 May 2010; revised 6 Jun 2010; accepted 6 Jun 2010; published 23 Jun 2010

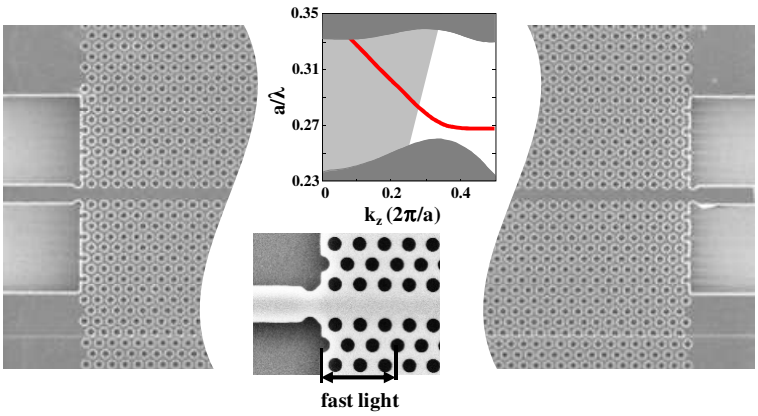

Fig. 1. Scanning Electron Microscope image of a single-row-missing PhCW. The wafer is composed of a series of twenty supposedly identical parallel waveguides etched into a Si-membrane. The top inset shows the dispersion diagram of the ideal waveguide, calculated for the geometric parameters actually measured on the device and for a 3.48 Si refractive index. The bottom inset represents an enlarged view of the injector [26] used for efficient coupling between the ridge-access waveguide and the PhCW.

Figure 2(a) shows two of the 18 measured transmission spectra. The transmission spectra are recorded by coupling TE-polarized light from a tunable external laser source (1520-1620 nm) via a polarization-maintaining fiber connected to a microlensed fiber. After passing through the device, the light emitted by the rear cleaved facet is collected by an infinity-corrected infrared objective (× 80, NA = 0.8) and its intensity is monitored by an InGaAs photodiode as the coherent source's wavelength is scanned [27].

In order to relate wavelengths to averaged group velocities, we also measure the group-index spectrum of every PhCW using an interferometric setup [28]. For 185a long waveguides, n_g values up to 120 can be recovered with a Fourier transform analysis of the interferograms. Figure 2(b) shows the $n_g(\lambda)$ curves recorded for every waveguide. For large n_g values, the recorded $n_g(\lambda)$ curves are not identical and present disorder-induced variations. In agreement with previous theoretical and experimental studies [17,19,29], the disorder is found to smear the band-diagram of the ideal waveguide at the boundary of the Brillouin zone. By averaging over the 18 samples the group index data for every wavelength, we infer an averaged $n_g(\lambda)$ relationship (solid black curve). The latter is used for relating wavelengths to average group velocities in the following.

3. Termination-less transmission spectra

The measured transmissions do not correspond to the so-called transmission in classical studies of the electronic (or photonic) transport of 1D electronic wires [12–14]. The actual spectra are contaminated by two effects, the reflection on the cleaved faced (this is specific to our design) and the reflection at the PhCW termination (this is inevitable). Although the later is critical, it is rarely considered in the literature and one often neglects its impact. In this Section, we describe our approach to derive "termination-less" transmission spectra from the measured ones.

3.1 Interpretation of the experimental data

Inspecting Fig. 2(a), we see that, for $\lambda<1556$ nm, the PhCW attenuation is negligible (5dB/cm) and the high-frequency oscillations are mostly Fabry-Perot fringes induced by the 30% reflectance of the cleaved facets. For $\lambda>1556$ nm ($n_g>25$), the transmission spectra exhibit two main features: a drop of the transmission and the presence of very large and rapid oscillations. This is consistently observed in all the recorded spectra. The drop is primarily attributed to the extrinsic losses of the PhCWs that are important for slow-light. In general, an increase of the attenuation is expected to produce a lowering of the Fabry-Perot-fringe

#128202 - $15.00 USD Received 10 May 2010; revised 6 Jun 2010; accepted 6 Jun 2010; published 23 Jun 2010

contrast induced by the reflection on the cleaved facet. But this is not what we observe: the recorded spectra exhibit intense and sharp peaks in the transmission, with small spectral linewidths ($Q = \lambda/\Delta\lambda \sim 20{,}000$) and with an intensity modulation that is even larger than that achieved at smaller wavelength with $n_g \approx 4$. One may naturally argue that the enhancement of the modulation contrast is due to the group-velocity impedance mismatch at the interface between the ridge-access waveguide and the PhCW, since this mismatch is known to result in an increased modal reflection that scales as $1-A(n_g)^{-1}$, where A is a constant factor.

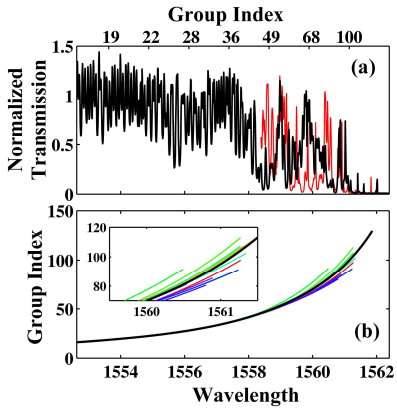

Fig. 2. Experimental data collected for the twenty PhCWs. **(a)** Spectra of two different waveguide instances (black and red curves). n_g dependence (top axis) is deduced from interferometric measurements **(b)** $n_g(\lambda)$ curves recorded for every waveguide. The large spreading at large n_g's (inset) results from disorder–induced fluctuations that smear the sharp cutoff at $v_g = 0$. The thick-black curve represents the ensemble-averaged curve used to relate the actual wavelength to an averaged group index.

Ideally, two independent requirements have to be met in practice at the PhCW interfaces. Firstly the coupling efficiency should be independent of n_g allowing a direct comparison between the energy transmitted at two different wavelengths. Secondly the backreflection should be as small as possible. We have carefully taken into account both requirements when designing the wafer by incorporating injectors with coupling efficiencies larger than 95% for $n_g<100$. The 5% losses are due mainly to out-of-plane scattering into the air-cladding. Thus backreflection is actually critically low, below 1% as shown by the 3D computational results in [26].

To further analyse the experimental data, we have performed fully-vectorial 3D calculations. These calculations include the light propagation into the access waveguide, the reflection on the cleaved facets, the coupling through the injector and the propagation in the 185a-long disordered PhCW section. Indeed, the difficult part consists in modeling the light transport through the PhCW. This is performed by using a recently developed approximate 3D coupled-Bloch-mode method [14,23]. In contrast to perturbation methods developed in earlier works [30–34], the present method takes into account important factors, such as out-of-plane leakage, in-plane multiple scattering inside a single hole and between holes, and localization effects that are virtually always present in 1D systems in the presence of multiple backscattering. The calculated data are shown in Fig. 3(a). They quantitatively reproduce all the salient features of the experimental curves in Fig. 2(a), in particular the transmission drop and the intense oscillations for large wavelengths.

The calculated spectrum has been obtained by assuming a size disorder model, in which only the hole radii of the two inner rows (these are the rows that are dominantly interacting with the waveguide mode field) are randomly and independently (distinct etched hole have fully-independent deformations) varied around their mean nominal value of 0.3a with a statistical Gaussian distribution of standard deviation $\sigma = 1.7$ nm, obtained by fitting the average value of the transmission (see the next Section). The disorder-model choice is

#128202 - $15.00 USD Received 10 May 2010; revised 6 Jun 2010; accepted 6 Jun 2010; published 23 Jun 2010

motivated for its simplicity, which allows us to carefully take into account multiple scattering effects between independent holes inside a single cell, and between different cells. The model is likely not to be highly accurate, since realistic deformation models should additionally include surface roughness and hole displacements. Indeed, our objective is not to provide a complete, fully-accurate and comprehensive modeling of light transport (this would require to perfectly know all the hole deformations over the 100-μm long PhCWs), but rather to use a generic tool that allows us to reproduce all the salient features of the measured spectra and to quantify the respective role of different mechanisms associated to the light transport. Although our model is simplistic (it relies on a single fitting parameter σ), we believe that it contains all the basic ingredients (out-of-plane loss, backscattering, multiple scattering) that are encountered in experiments. This statement is additionally confirmed by the comparison of the numerical spectra in Fig. 3 with the experimental ones in Fig. 4. The agreement is very good on overall, despite the fact that the resonance peaks and spikes are not located at the same spectral positions (this would require a perfect knowledge of the deformation).

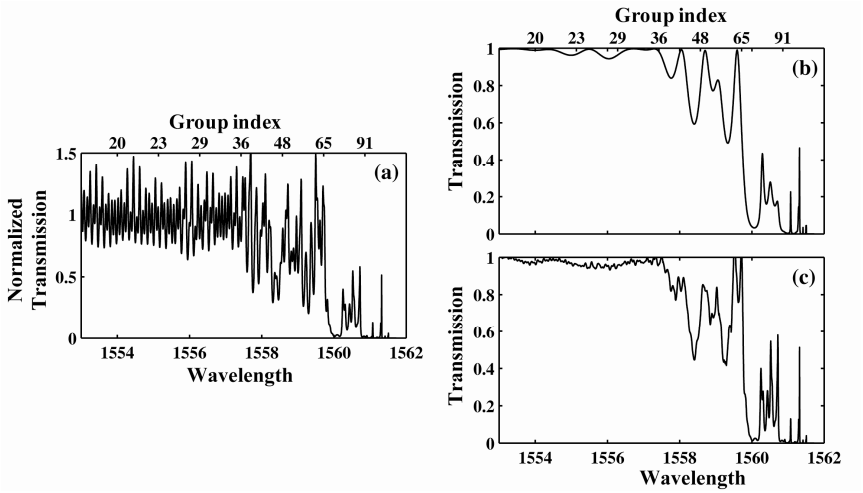

Fig. 3. Test of the median-filter method with purely-calculated transmission spectra. **(a)** Typical transmission spectrum calculated by including light injection from the ridge to the PhCW and multiple-reflection on the ridge cleaved facets. **(b)** Termination-less transmission spectrum obtained by directly calculating the transmission of the disordered PhCW used for the calculation in **(a)**. **(c)** Transmission spectrum obtained by filtering the curve in **(a)**. Although the filtering process is imperfect, it provides reliable estimates for the termination-less transmission.

The curve in Fig. 3(b) shows the transmission spectrum obtained by calculating the transmittance through the 185*a*-long PhCW alone with the same disorder instance. In this "*termination-less*" spectrum that is free from any spurious back-reflections at the access–ridge facets or at the ridge-PhCW interfaces, it is remarkable that the transmission drop is again assisted by rapid and sharp oscillations, with Q values comparable to the experimental ones. This provides a firm confirmation that the experimental oscillations at long wavelengths [Fig. 2(a)] are intrinsically due to the fabrication imperfections, and not to any spurious backscattering introduced by termination facets.

3.2 Post-processing the experimental transmission spectra

Because of the high reflectance at the cleaved facets, the experimental transmission spectra have been processed before further analysis. The processing is achieved with a median filter with a frequency-dependent window that depends on the local group index of the analyzed data. Before being applied to the experimental data, the processing technique has been first validated with the numerical data. Figure 3(c) shows the filtered transmittance spectrum obtained by applying the median filter to the numerical data of Fig. 3(a). As shown, the

#128202 - $15.00 USD Received 10 May 2010; revised 6 Jun 2010; accepted 6 Jun 2010; published 23 Jun 2010

filtering largely smoothes the Fabry-Perot oscillations for $n_g \leq 10$, but preserves the sharp peaks for larger n_g's.

Figures 4(a) and 4(c) show two experimental spectra [they are identical to those previously shown in Fig. 2(a)] and the associated filtered spectra, see Figs. 4(b) and 4(d). The insets show two intense peaks obtained from the filtered spectra. Both of them exhibit Q values of ≈20,000, just like in the theoretical data of Figs. 3(b) or 3(c). Finally, let us note that the theoretical spectra for the termination-less or for the filtered cases share the same characteristics as those of the filtered experimental spectra.

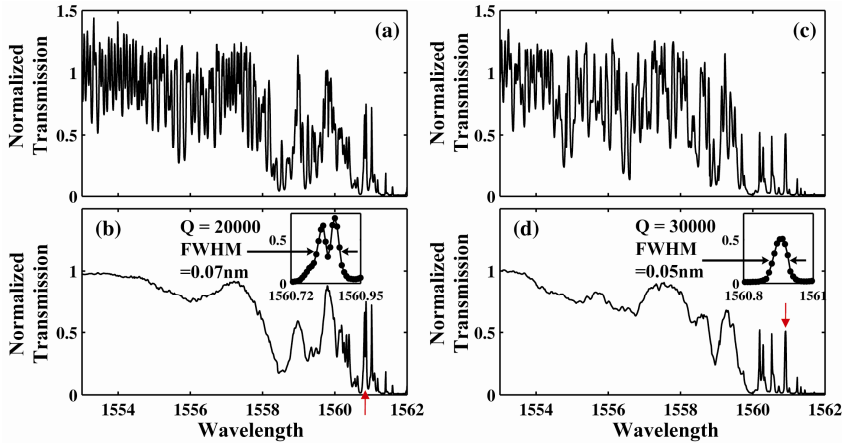

Fig. 4. Examples of experimental filtered spectra **(b)** and **(d)** used in the following statistical analysis. The corresponding measured spectra are shown in **(a)** and **(c)**. The red arrows point at the spectral locations of the insets. Note the important similarities between the filtered spectra and the theoretical spectra of Figs. 3(b) and 3(c).

4. Probability density function for the transmission

Let us first consider ensemble-averaged quantities over the 18 waveguides. After filtering, ensemble-averaged quantities, denoted by <•>, are first calculated using classical statistical treatments. Note that the averaging is performed for a fixed wavelength. We then use the black curve in Fig. 2(b) to relate the wavelength to an average group-index. Figure 5 shows the n_g-dependence of the averaged transmission <T>. The ensemble-averaged experimental data (thick-black curve) quantitatively agree with the theoretical data (red curve) obtained by averaging 1000 *termination-less* transmission spectra for random independent disorder realizations with the same disorder level σ = 1.7 nm. As shown in the inset, the value σ = 1.7 nm is chosen because it offers the best fit with the experimental data. We regard this value as reasonably acceptable in view of [25], where the authors analyse 30 high-resolution SEM pictures of e-beam written PhCWs of various material and report standard deviations between 1.5 and 3.5 nm depending on the different materials and fabrication techniques. The case <T> = 0.5 is conceptually important as it marks the transition between the ballistic and localization regimes [15] ($L \approx l_c$, strictly speaking, $L = l_c$ corresponds to <T> = 1/e) and practically interesting as it offers a reasonable compromise between delay and losses.

#128202 - $15.00 USD Received 10 May 2010; revised 6 Jun 2010; accepted 6 Jun 2010; published 23 Jun 2010

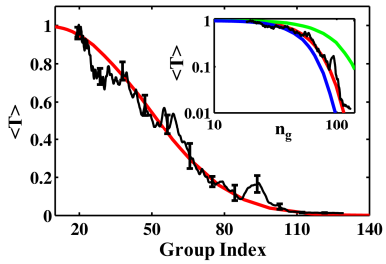

Fig. 5. Comparison between the experimental results (black) and the model predictions (red) for the averaged transmission <T>. The experimental ensemble–averages are collected over N = 18 independent realizations. Those of the theoretical data are collected over 1000 independent realizations with σ = 1.7 nm. The vertical bars represent the statistical error $\sigma_T/N^{1/2}$. The inset is a log-log representation for different values of the standard deviation of the hole diameter, σ = 1 nm (green), σ = 1.7 nm (red), σ = 2 nm (blue).

Figure 6 compares 18-bin experimental histograms gathered at different group velocities that correspond to <T> = 0.9, 0.5 and 0.1 with the theoretical probability density function P(T) (red curve). Note that, like the theoretical curves obtained by collecting 5.10^5 independent disorder realizations, are normalized such that $\int_{[0;1]} P(T)dT = 1$. Again the agreement is quantitative. Both the experimental and computational data predict a very large standard deviation ($\sigma_T^2 = \langle T^2\rangle - \langle T\rangle^2$), $\sigma_T \approx 0.28$, a value which is actually comparable with the standard deviation $1/(12)^{1/2} = 0.288$ of a uniform distribution with equidistributed values in the interval [0 1]. This probability density function broadening is a direct consequence of the presence of peaks in the transmission spectra of Figs. 2, whose resonant frequencies vary from one realization to another.

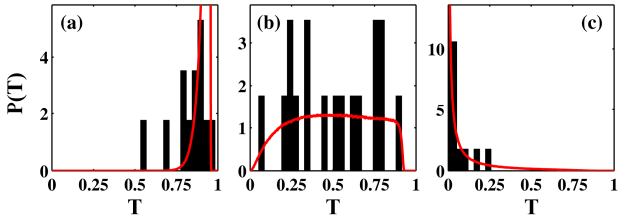

Fig. 6. Histograms (black bars) of the 18 values of the transmission for <T> = 0.9 **(a)**, <T> = 0.5 **(b)** and <T> = 0.1 **(c)**. The red curves are the corresponding calculated probability density function obtained by collecting 5.10^5 independent disorder realizations at the corresponding n_g's, n_g = 25 **(a)**, 55 **(b)** and 90 **(c)**. The bar width of the experimental data is ΔT = 0.05 and the bar heights are normalized such that $\Sigma_p P_p(T)\Delta T = 1$, to allows us for a direct comparison with the theoretical data.

5. Field pattern at peak transmission

To further understand the properties of the slow-light transport around <T>≈0.5, let us examine the field pattern in the PhCW. In the coupled-Bloch mode formalism [14,23], the electromagnetic field in the PhCW is expressed as a superposition of the backward- and forward-propagating fundamental Bloch modes, which exchange their energy and which scatter in the air clad as they propagate along the *z*-direction. Let us denote by $c^+(z)$ and $c^-(z)$ the excitation coefficients of the fundamental forward- and backward-propagating Bloch modes, and let us normalized these Bloch modes such that the flux of the *z*-component of their Poynting vector across a transverse surface are unitary. Thus $|c^+(z)|^2$ and $|c^-(z)|^2$ represent the local energy flowing in the positive and negative z-directions in the PhCW.

#128202 - $15.00 USD Received 10 May 2010; revised 6 Jun 2010; accepted 6 Jun 2010; published 23 Jun 2010

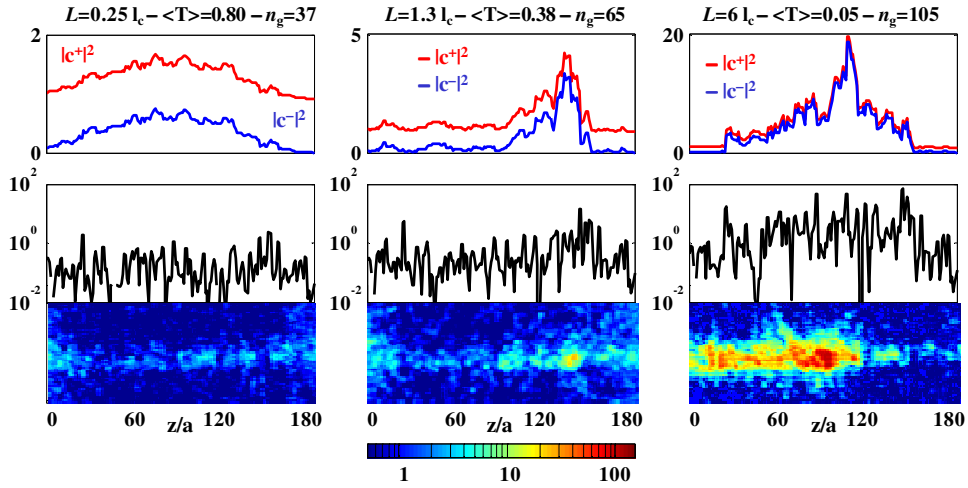

Fig. 7. Field pattern inside a 185-a-long PhCW for the ballistic (left, $n_g \approx 40$, $L \approx 0.25 l_c$), intermediate (middle, $n_g \approx 65$, $L \approx 1.3 l_c$) and localization (right, $n_g \approx 105$, $L \approx 6 l_c$) regimes. Top: Calculated data for termination-less PhCW showing the forward- and backward-propagating Bloch mode intensities, $|c^+(z)|^2$ (red) and $|c^-(z)|^2$ (blue). Note the changes of the vertical axes. Middle: The calculated out-of-plane losses, $\partial(|c^+|^2-|c^-(z)|^2)/\partial z$ (black). Bottom: Far-field patterns obtained by imaging the sample surface onto an IR-camera. Note that since the experimental and theoretical data do not correspond to the same disorder instance, the spike locations in the black curves and in the images are not expected to be identical. In all graphs, light is incoming from the left side. Note that the color scale is logarithmic.

$|c^+(z)|^2$ and $|c^-(z)|^2$ are respectively shown with the red and blue curves in the top part of Fig. 7. They are calculated with the coupled-Bloch mode formalism for *termination-less* 185*a*-long disordered PhCWs illuminated from the left side ($z = 0$) with a unitary excitation, $c^+(0) = 1$ and $c^-(L) = 0$. The curves are gathered for specific resonance wavelengths corresponding to intense transmission peaks ($|c^+(L)|^2 \approx 1$). With many calculations obtained for different realizations of disorder, we have verified that these peaks occur for typical field patterns in the waveguide. The chosen examples represent normal behaviors of the field pattern rather than the exception.

Perfect transport for disorder-free PhCWs would correspond to $c^+(z) = 1$ and $c^-(z) = 0$ for any z, a situation that is roughly observed for the ballistic transport regime obtained for <T> = 80% ($L = 0.25\ l_c$, $n_g \approx 37$) and shown in the upper-left side of Fig. 7. As n_g increases, backscattering becomes the dominant mechanism for loss. The field pattern becomes an intense and almost stationary pattern (it would be perfectly-stationary in the absence of out-of-plane losses), of which maximum intensities rapidly grow as n_g increases. For <T> = 50% ($L = l_c$, $n_g \approx 65$), the intensity of the back-reflected Bloch mode may locally be 5-times larger than the incident intensity. This is a remnant of a delocalized Fabry-Perot-like resonance induced by a distributed back-reflection with fixed boundary conditions, $|c^+(0)|^2 = 1$ and $|c^-(L)|^2 = 0$. As one moves to slightly larger n_g's, backscattering becomes much stronger than out-of-plane losses and one enters the localization regime. The stationary-field becomes stronger and this enhancement is accompanied by the emergence of localized states evidenced by the rapid spatial variations of $|c^+|^2$ or $|c^-|^2$ at <T> = 5% ($L = 6 l_c$). As shown by other calculations, the latter are due to the formation of short (but efficient) reflective sections in the PhCW. Thus in addition to the Fabry-Perot extended resonance, the transport is assisted by the formation of a series of localized states that are coupled to each other and that we are inclined to interpret as the necklace states [35,36] initially proposed in [37] to explain the observation of full transmission of electrons in 1D disordered systems.

#128202 - $15.00 USD Received 10 May 2010; revised 6 Jun 2010; accepted 6 Jun 2010; published 23 Jun 2010

These theoretical predictions are not easy to evidence experimentally, since the coupled-mode coefficients are connected to guided waves that are bound to the structure. They can however be indirectly checked by considering that the spatial derivative of the net energy flow, $\partial(|c^+|-|c^-|)/\partial z$ [38], is a related quantity that represents the out-of-plane leakage rate (for absorption-free materials) and that is easily measured experimentally. The calculated loss patterns are shown in arbitrary units with the black curves in the middle part of Fig. 7. There are two common important features. Firstly, the curves are all spiky, with a large (two order of magnitude is typical) modulation showing that the out-of-plane losses strongly vary from one cell to the other. Secondly, the out-of-plane losses rapidly increase with n_g, a 50-fold enhancement being predicted as <T> decreases from 80% (left) to 5% (right).

The existence of these spiky patterns has been quantitatively confirmed by recording the far-field images of the PhCW out-of-plane losses, using an infinity-corrected infrared objective (× 80, NA = 0.9) to image the sample surface on an IR-camera. The images, which have been gathered under the same conditions as the theoretical ones for wavelengths corresponding to transmission peaks and for similar n_g values, are shown in the lower part of Fig. 7; they quantitatively confirm all the salient features of the theoretical predictions, including the spiky profile, the existence of PhCW sections with weak losses even at large n_g's and the rapid increase of the peak-intensity of the spikes and of their contrast with n_g.

6. Conclusion

The prime requirement on photonic materials is that they exhibit low loss, or that at least the loss is sufficiently well characterized that it can be compensated appropriately. The fibre optic network, where 10s of dB of loss are commonly compensated with amplifiers, is a typical example. Slow light materials based on natural or artificial resonances are assumed to follow similar rules. Here, we have shown that this determinism is only true in the ballistic transport regime.

Even for relatively small waveguide lengths (L = 100-200a) and group indices ($n_g \approx 50$) operating at the border between the ballistic and the localization regimes, the slow-light transport in real PhCWs strongly departs from the perfect Bloch-mode propagation in periodic systems. Because of the enhanced distributed backscattering evidenced by the ratio of the c^+ and c^- coefficients, we have shown that the field-pattern contains a substantial back-propagating component that is larger than the incident field itself, which may be understood as an extended stationary mode rather than as a propagating slow Bloch mode. The standard single-row-missing PhCW geometry studied here is only one specific (and not necessarily the best) candidate for slow-light circuitry, but we believe that the present results also apply more generally to corrugated waveguides (or coupled-cavity [39]) operated in a regime for which backscattering is the dominant loss mechanism. This highlights the need for developing new designs of slow light waveguides with a lower backscattering coefficient; if the attenuation is dominated by out-of-plane scattering, localization will not occur and the simple picture of slow light as a slowly propagating Bloch mode will indeed apply. Alternatively, the strong build-up shown in Fig. 7 may be beneficial for nonlinear optics or lasing applications [1].

Acknowledgments

This research is supported under the European contract SPLASH of the 6th EU Framework program. Simon Mazoyer thanks the DGA for financial support. This work is part of the research program of FOM, which is financially supported by NWO. M. S. acknowledges the support of the European Community under the Marie Curie Scheme (Contract No. MEST-CT-2005-021000).

#128202 - $15.00 USD Received 10 May 2010; revised 6 Jun 2010; accepted 6 Jun 2010; published 23 Jun 2010